

赣南陶锡坑钨矿床 He-Ar 同位素地球化学研究*

宋生琼^{1,2} 潘力川¹ 魏文凤^{1,3}

SONG ShengQiong^{1,2}, PAN LiChuan¹ and WEI WenFeng^{1,3}

1. 中国科学院地球化学研究所 矿床地球化学国家重点实验室, 贵阳 550081

2. 贵州省国土资源勘测规划研究院, 贵阳 550005

3. 成都理工大学地球科学学院, 成都 610059

1. State Key Laboratory of Ore Deposit Geochemistry, Institute of Geochemistry, Chinese Academy of Sciences, Guiyang 550081, China

2. Guizhou Land Survey & Plan Institute, Guiyang 550005, China

3. College of Earth Sciences, Chengdu University of Technology, Chengdu 610059, China

2018-08-02 收稿, 2018-11-16 改回.

Song SQ, Pan LC and Wei WF. 2019. He and Ar isotopes of ore-forming fluids in the Taoxikeng tungsten deposit, southern Jiangxi Province, China. *Acta Petrologica Sinica*, 35(1): 243–251, doi:10.18654/1000-0569/2019.01.19

Abstract China accounts for about 60% tungsten reserves of the world. More than 90% of the Chinese tungsten resources occur in the Nanling region as tungsten polymetallic deposits. The Nanling region locates at the central west Cathaysia Block in South China where abundant Jurassic granitic intrusions are distributed. Previous studies have significantly advanced our understanding of the tungsten ore formation in the Nanling region. These deposits are usually of the quartz-wolframite vein type. They have ages of about 150 ~ 160Ma, and are spatially and temporally related to the Jurassic granites, believed to be produced by crustal anatexis. The formation of quartz-vein type tungsten deposits in South China has always been considered to be related to S-type granite derived from remelting of crustal materials. However, in recent years, studies on the metallogenic mechanism of Mesozoic W-Sn deposits in Nanling region have demonstrated that mantle material and mantle fluid may be involved in tungsten and tin mineralization. The Taoxikeng deposit is a large-sized W deposit located at Jiangxi. Here, we conducted studies He and Ar isotope of pyrite- and arsenopyrite-trapped fluid inclusions on Taoxikeng quartz-vein type wolframite deposit. The analytical results of He and Ar isotope of pyrite- and arsenopyrite-trapped fluid inclusions show that, $^3\text{He}/^4\text{He}$ ratio of arsenopyrite between 1.38 and 2.11Ra (Ra is $^3\text{He}/^4\text{He}$ in air, $1\text{Ra} = 1.39 \times 10^{-6}$). The $^3\text{He}/^4\text{He}$ of pyrite between 0.67 and 0.37Ra. The concentration of ^4He is between 1.98×10^{-7} and $49.1 \times 10^{-7} \text{cm}^3 \text{STP/g}$. The concentration of ^{40}Ar is $4.19 \times 10^{-7} \sim 51.4 \times 10^{-7} \text{cm}^3 \text{STP/g}$, $^3\text{He}/^4\text{He}$ is 0.37 ~ 2.11Ra. $^{40}\text{Ar}/^{36}\text{Ar}$ is 309.5 ~ 383.6, slightly higher than the ratio of atmosphere $^{40}\text{Ar}/^{36}\text{Ar}$ (295.5), the ratio of $^{38}\text{Ar}/^{36}\text{Ar}$ is 0.19 ~ 0.23, with the average of 0.183, which is close to the atmospheric value (0.188). These indicate that the ore-forming fluid has the characteristics of mixing both ends of the crust and mantle. The crustal fluid is composed of low temperature atmospheric water interacted with crustal rocks, and the fluid containing mantle-derived components is exsolved from granite. Combined with previous studies, it is believed that the deposit is closely related to Mesozoic large-scale asthenosphere upwelling, lithospheric thinning and crustal extension in South China, which provided favorable condition to lead the mantle-derived He/heat upward and then to melt the crustal materials and to form the ore-forming granitic magmas.

Key words Taoxikeng tungsten deposit; Fluid inclusions; He and Ar isotopes; S-type granites; Mantle-derived component

摘要 华南石英脉型黑钨矿的形成一直被认为是与地壳沉积物质重熔形成的 S 型花岗岩有关。然而,近年来对南岭中生代成岩成矿机制的研究发现,地幔组分可能参与了钨、锡成矿作用。本文对陶锡坑石英脉型钨多金属矿床与黑钨矿共生的黄铁矿和毒砂中流体包裹体的 He、Ar 同位素进行了研究。结果显示,上述矿物中流体包裹体的 $^3\text{He}/^4\text{He}$ 值为 0.37 ~ 2.11Ra (Ra 为空气的 $^3\text{He}/^4\text{He}$ 值, $1\text{Ra} = 1.39 \times 10^{-6}$), 介于地幔与地壳的 $^3\text{He}/^4\text{He}$ 值之间; $^{40}\text{Ar}/^{36}\text{Ar}$ 值为 309.5 ~ 383.6, 平均 335.4,

* 本文受中科院战略性先导科技专项(XDB18000000)和国家“973”项目(2007CB411400)联合资助。

第一作者简介: 宋生琼,女,1983年生,博士,副研究员,主要从事矿床地球化学研究, E-mail: 156160493@qq.com

略高于大气的 $^{40}\text{Ar}/^{36}\text{Ar}$ 比值(295.5)。研究表明,成矿流体具有壳-幔两端元混合的特征。其中,地壳端元的流体为经过地下循环的低温饱和大气水,地幔端元的流体为矿区隐伏花岗岩体成岩过程中分异出的岩浆流体。结合前人研究成果,认为该矿床的形成与华南中生代燕山期发生的软流圈上涌、岩石圈减薄、地壳伸展等地球动力学作用有密切联系。这种动力学过程为地幔组分带来的热引起地壳沉积物质重熔形成钨多金属成矿花岗岩浆提供了条件。

关键词 淘锡坑钨矿床; 流体包裹体; He 和 Ar 同位素; S 型花岗岩; 地幔组分

中图法分类号 P597.2; P618.67

成矿流体是地质流体在特定地质环境中经过特定的演化阶段形成的特征产物,绝大多数金属矿产的形成都与成矿流体的活动有着非常密切的关系。长期以来,石英脉型黑钨矿一直被认为是与同碰撞背景之下陆壳重熔的 S 型花岗岩有关,成岩和成矿过程仅有地壳流体参与,而少有深部或地幔物质参与成矿作用(刘义茂等,1998; 毛景文等,2004; 张文兰等,2006; 丰成友等,2007; 魏绍六等,2006)。然而,近年来对南岭中生代成岩成矿机制的研究发现,地幔物质和地幔流体可能参与了钨、锡成矿作用(涂光炽,1998; 赵振华等,2000; 马铁球等,2005; 席斌斌等,2008; Wu *et al.*, 2011; Hu *et al.*, 2012)。流体包裹体是矿物在生长过程中保留下来最完整和最直接的原始样品,对流体包裹体进行研究是获取成矿流体信息最直接、最有效的手段(Roedder, 1984; Graupner *et al.*, 1999, 2001; Wilkinson, 2001; Paradis *et al.*, 2004; 卢焕章等,2004; 池国祥和赖健清,2009)。因地幔不同圈层的 He 同位素组成不同且相差很大,典型地幔流体中的 He 同位素,其 $^3\text{He}/^4\text{He}$ 比值为 $7\sim 9\text{Ra}$ ($\text{Ra} = 1.39 \times 10^{-6}$, 为大气成因稀有气体的 $^3\text{He}/^4\text{He}$ 比值),地壳成因 He 同位素的 $^3\text{He}/^4\text{He}$ 为 $0.01\sim 0.05\text{Ra}$,地壳与地幔 $^3\text{He}/^4\text{He}$ 比值相差近 1000 倍(Torgersen and Jenkins, 1982; Hu *et al.*, 1998, 2009; Burnard *et al.*, 1999; 胡瑞忠等,1999)。只要成矿流体中有少量地幔流体的加入,就会使成矿流体的 $^3\text{He}/^4\text{He}$ 比值发生很大变化。因此,热液矿床 He 同位素组成的研究能很好地示踪成矿流体中是否有地幔流体的加入(Stuart *et al.*, 1995; Burnard *et al.*, 1999; Hu *et al.*, 2004, 2009; Li *et al.*, 2007)。相反地, ^{36}Ar 在幔源流体中的含量很低,因此 $^{40}\text{Ar}/^{36}\text{Ar}$ 的比值可以很好的示踪岩浆流体中低温海水或大气水的加入。因此,同一样品中 He、Ar 同位素的组成能够相互补充,以示踪成矿流体中的地幔流体、低温海水或大气水及其混合作用(Burnard and Polya, 2004)。

淘锡坑钨矿床位于江西省崇义县西南 9km 处,属于大型石英脉型钨多金属矿床(徐敏林等,2006)。以往对该矿床的研究主要集中在成矿地质特征、成矿物质来源及成岩成矿时代等方面(徐敏林等,2006; 邹欣,2006; 陈郑辉等,2006; 郭春丽等,2007, 2008; 吴至军等,2009; 宋生琼等,2009, 2011a, b; Guo *et al.*, 2011; 杨帆等,2014)。对成矿流体的来源及演化等问题研究较少,矿床成矿机制也未得到深入研究。稀有气体同位素对示踪成矿流体的形成演化具有重要意义。因此,本文通过对淘锡坑钨多金属矿床主成矿期毒砂和黄铁矿中流体包裹体 He、Ar 同位素进行研究,探讨矿

床成矿流体的来源、演化及其成矿机理。

1 地质背景

华南陆块由扬子克拉通和华夏地块在新元古代沿江南造山带碰撞拼贴而形成(Zhang and Zheng, 2013),华南陆块与华北陆块在三叠纪沿秦岭-桐柏-红安-大别-苏鲁造山带碰撞拼贴形成统一的中国东部大陆(Wu and Zheng, 2013)。华夏地块的基底为前寒武纪变质岩,盖层为志留纪至中生代的沉积岩地层(Yu *et al.*, 2005)。华夏地块以中生代强烈的花岗岩浆活动和与其相关的 W-Sn 多金属大规模成矿闻名于世,相关的成岩、成矿作用大致可以分为约 230~200Ma、160~150Ma 和 100~80Ma 三个时期(Hu and Zhou, 2012; Mao *et al.*, 2013; 胡瑞忠等,2015; Yuan *et al.*, 2008, 2011, 2015)。

淘锡坑钨多金属矿床位于华夏地块南岭地区的江西省崇义县境内,北北东向九龙脑-营前岩浆岩带与东西向古亭-赤土构造带的交汇部位(图 1)。NE 向和 EW 向区域性断裂,为本区燕山期成矿花岗岩体以及钨多金属矿床的形成提供了有利的构造条件。

淘锡坑钨多金属矿床及邻区主要出露九龙脑复式花岗岩体,岩体形成时代为加里东期和燕山期,其中以后者为主。燕山期岩体主要为黑云母、二云母和白云母花岗岩,锆石 U-Pb 年龄为 $158.7 \pm 3.9\text{Ma}$ 和 $157.6 \pm 3.5\text{Ma}$ (郭春丽等,2007)。区内广泛出露震旦-奥陶系地层,另有少量泥盆系、石炭系、二叠系、侏罗系、白垩系和第三系地层分布。淘锡坑钨多金属矿床产于隐伏花岗岩体的内外接触带,钻孔揭露的岩性为细粒白云母花岗岩和中细粒黑云母花岗岩。岩体的 SiO_2 含量为 73%~78%, Al_2O_3 为 12%~15%, $\text{K}_2\text{O} + \text{Na}_2\text{O}$ 含量为 6.3%~8.2%, $\text{K}_2\text{O}/\text{Na}_2\text{O} > 1$, $\text{A}/\text{CNK} > 1.1$,属于强过铝质钙碱性系列的 S 型花岗岩(吴至军等,2009; 邹欣,2006)。

淘锡坑钨多金属矿床主要产于隐伏花岗岩体的外接触带,为石英脉型矿床。近地表矿脉细小密集,往下脉体变宽变少,再向下至岩体内逐渐尖灭,相应 WO_3 品位也由浅部向深部有变富的趋势。矿脉延深大,部分矿脉深度大于长度,矿床平均品位较富, WO_3 平均达 2.6%(徐敏林等,2006)。垂向上矿化主要富集于岩体顶部往上 100~400m 范围内,而花岗岩体顶部附近的矿化变弱。

矿石中主要金属矿物有黑钨矿、黄铜矿、黄铁矿、锡石、

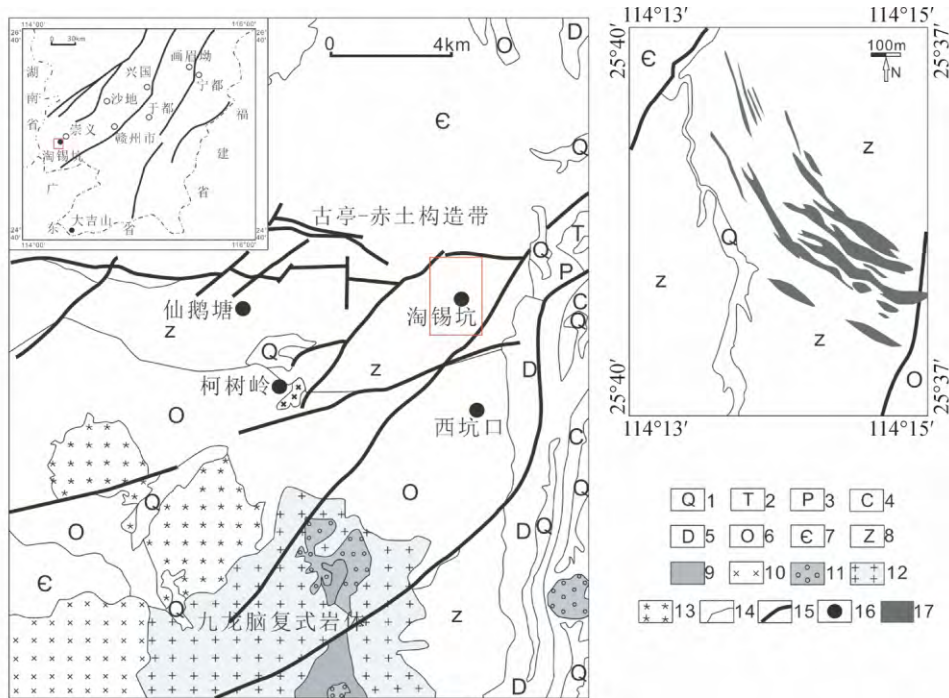


图1 淘锡坑矿床及其区域地质简图(据徐敏林等,2006)

1-第四系粘土;2-三叠系砂岩;3-二叠系砂岩;4-石炭系灰岩;5-泥盆系页岩;6-奥陶系板岩;7-寒武系板岩;8-震旦系复理石火山质泥砂岩;9-晚侏罗世细粒斑状黑云母花岗岩;10-晚侏罗世中细粒斑状二云母花岗岩;11-晚侏罗世中细粒斑状黑云母花岗岩;12-中侏罗世细粒斑状黑云母花岗岩;13-早志留世中粒含斑花岗闪长岩;14-地层界线;15-断裂;16-钨锡矿床;17-矿体

Fig. 1 A regional geological sketch map of the Taosikeng tungsten deposit (modified after Xu *et al.*, 2006)

白钨矿、闪锌矿、辉钼矿、毒砂和辉铋矿。非金属矿物有石英、黄玉、萤石、白云母、铁锂云母、电气石、方解石、叶腊石、绿泥石和绢云母等。次生矿物主要有铜蓝、高岭土和褐铁矿。垂向上矿物组合具“逆向”分带特征,近地表或矿体上部为黑钨矿-锡石带,中部为黑钨矿-黄铜矿带,下部为黑钨矿-辉钼矿带,深部还见萤石-辉铋矿-方解石等低温矿物。陈郑辉等(2006)获得该矿床辉钼矿的 Re-Os 等时线年龄为 $156.4 \pm 3.5 \text{ Ma} \sim 153.5 \pm 2.2 \text{ Ma}$,与区内燕山期花岗岩的锆石 U-Pb 年龄(郭春丽等,2007)在误差范围内一致,指示钨矿与花岗岩具有密切的时、空及成因联系。

2 样品采集与测试方法

本次 He、Ar 同位素研究的样品均采自淘锡坑钨多金属矿床地下坑道 056 到 356 中段的石英大脉中。在野外和室内研究的基础上,选取与黑钨矿共生的自形、半自形黄铁矿颗粒和短柱状且柱面具纵纹的毒砂颗粒作为测试样品(图 2)。这些黄铁矿和毒砂显微镜下晶形完整,未见后期改造的痕迹,其中的流体包裹体绝大多数为原生包裹体,其组成和性质代表了成矿流体的组成和性质。

在双目镜下挑选新鲜纯净的黄铁矿、毒砂,纯度达 99% 以上,在中国科学院地球化学研究所矿床地球化学国家重点

实验室的稀有气体质谱实验室进行 He 和 Ar 同位素测定。实验步骤如下:(1) 将挑选好的单矿物在超声波丙酮溶液中洗净烘干;(2) 称取 500 ~ 1000mg 矿物样品装入螺旋式压碎装置;(3) 加热烘烤螺旋式压碎装置及其中的样品,烘烤温度在 120 ~ 150°C 之间,除掉矿物和装置吸附的大气成分,并把系统抽成高真空状态;(4) 在高真空条件下压碎样品,释放矿物中的流体包裹体,然后进入气体净化系统纯化 He 和 Ar;(5) 将纯化分离后的 He 和 Ar 先后送入质谱中进行 He、Ar 同位素分析。分析仪器为英国产 GV5400He 型静态真空稀有气体质谱仪, ^3He 用电子倍增器接收, ^4He 用法拉第杯接收。仪器的主要技术参数为:灵敏度 He 为 $2.9796 \times 10^6 \text{ A/Pa}$,Ar 为 $8.2642 \times 10^6 \text{ A/Pa}$,分辨率电子倍增器为 682.3,法拉第杯为 228。

3 He、Ar 同位素测试结果

黄铁矿和毒砂流体包裹体的 He、Ar 同位素测试结果见表 1。结果显示,毒砂的 $^3\text{He}/^4\text{He}$ 比值为 1.38 ~ 2.11Ra (Ra 为空气的 $^3\text{He}/^4\text{He}$ 值, $1\text{Ra} = 1.39 \times 10^{-6}$),黄铁矿的 $^3\text{He}/^4\text{He}$ 为 0.37 ~ 0.67Ra。 ^4He 的浓度为 $1.98 \times 10^{-7} \sim 49.1 \times 10^{-7} \text{ cm}^3 \text{ STP/g}$, ^{40}Ar 的浓度为 $4.19 \times 10^{-7} \sim 51.4 \times 10^{-7} \text{ cm}^3 \text{ STP/g}$, $^{40}\text{Ar}/^{36}\text{Ar}$ 为 309.5 ~ 383.6,略高于大气中 $^{40}\text{Ar}/^{36}\text{Ar}$ 比值

表1 淘锡坑钨矿床毒砂、黄铁矿中流体包裹体的氦、氩同位素组成

Table 1 He and Ar isotopic compositions of fluid inclusions trapped in pyrite and arsenopyrite from the Taosikeng tungsten deposit

样品号	矿物	压碎次数	重量	^4He (cm^3STP)	^{40}Ar (cm^3STP)	$^3\text{He}/^4\text{He}$ (Ra)	$^{38}\text{Ar}/^{36}\text{Ar}$	$^{40}\text{Ar}/^{36}\text{Ar}$	$^{40}\text{Ar}^*/^4\text{He}$	^4He ($\text{cm}^3\text{STP/g}$)	^{40}Ar ($\text{cm}^3\text{STP/g}$)	F^4He
TB056-17-1	毒砂	1		2.62×10^{-8}	6.29×10^{-8}	1.25 ± 0.02	0.26 ± 0.02	306.4 ± 12	0.044			
		2		2.61×10^{-8}	4.79×10^{-8}	1.51 ± 0.03	0.25 ± 0.03	313.5 ± 11	0.075			
		Total	0.2645	5.23×10^{-8}	1.11×10^{-7}	1.38	0.23	309.5	4.19×10^{-7}	0.060	1.98×10^{-7}	4.19×10^{-7}
TF306-30-2-1	毒砂	1		2.68×10^{-7}	1.80×10^{-7}	2.09 ± 0.01	0.19 ± 0.01	336.1 ± 5	0.079			
		2		2.82×10^{-8}	4.78×10^{-8}	2.12 ± 0.03	—	321.7 ± 19	0.189			
		Total	0.0784	2.97×10^{-7}	2.28×10^{-7}	2.09	0.19	333.1	29.1×10^{-7}	0.089	37.8×10^{-7}	29.1×10^{-7}
TF356-33-1-1	毒砂	1		1.21×10^{-7}	1.26×10^{-7}	2.00 ± 0.02	0.19 ± 0.01	323.2 ± 6	0.086			
		2		2.76×10^{-7}	1.28×10^{-7}	2.16 ± 0.02	0.18 ± 0.01	343.0 ± 6	0.068			
		Total	0.1951	3.97×10^{-7}	2.54×10^{-7}	2.11	0.19	333.2	13.0×10^{-7}	0.075	20.4×10^{-7}	13.0×10^{-7}
TF356-30-1	毒砂	1		1.18×10^{-7}	8.77×10^{-8}	1.8 ± 0.01	0.2 ± 0.01	333.2 ± 12	0.066			
		2		1.99×10^{-7}	4.55×10^{-8}	1.89 ± 0.01	—	499.9 ± 26	0.09			
		Total		3.17×10^{-7}	1.33×10^{-7}	1.86	0.2	383.6	6.65×10^{-7}	0.082	15.8×10^{-7}	6.65×10^{-7}
TF356-37-2	毒砂	1		5.50×10^{-7}	7.81×10^{-7}	1.46 ± 0.01	0.19 ± 0.01	316.0 ± 0.6	0.087			
		2		3.98×10^{-7}	2.12×10^{-7}	1.53 ± 0.01	0.19 ± 0.01	365.3 ± 4	0.094			
		Total		9.49×10^{-7}	9.92×10^{-7}	1.49	0.19	326.5	51.4×10^{-7}	0.09	49.1×10^{-7}	51.4×10^{-7}
TL256-5-1-1	黄铁矿	1		8.25×10^{-8}	1.16×10^{-7}	0.68 ± 0.01	0.19 ± 0.01	321.5 ± 7	0.082			
		2		5.07×10^{-8}	8.53×10^{-8}	0.65 ± 0.01	0.19 ± 0.02	326.0 ± 9	0.090			
		Total	0.1651	1.33×10^{-7}	2.01×10^{-7}	0.67	0.19	323.4	12.2×10^{-7}	0.085	8.07×10^{-7}	12.2×10^{-7}
TF306-30-1-1	黄铁矿	1		2.81×10^{-7}	8.79×10^{-8}	0.25 ± 0.01	0.19 ± 0.02	318.2 ± 6	0.014			
		2		2.13×10^{-7}	8.06×10^{-8}	0.52 ± 0.01	0.19 ± 0.02	361.1 ± 11	0.066			
		Total	0.1965	4.94×10^{-7}	1.68×10^{-7}	0.37	0.19	338.7	8.57×10^{-7}	0.036	25.1×10^{-7}	8.57×10^{-7}

注:因表格空间不够,有关各同位素的含量及其浓度未列出误差; $^{40}\text{Ar}^*$ 表示扣除空气 ^{40}Ar 后的放射成因氩;样品重量是指样品被压碎至小于100目的部分;表中 ^4He 和 ^{40}Ar 的“浓度”是指每克寄主矿物中包裹体内的稀有气体量,它是流体包裹体中稀有气体真实浓度的粗略衡量标准. 浓度误差小于1

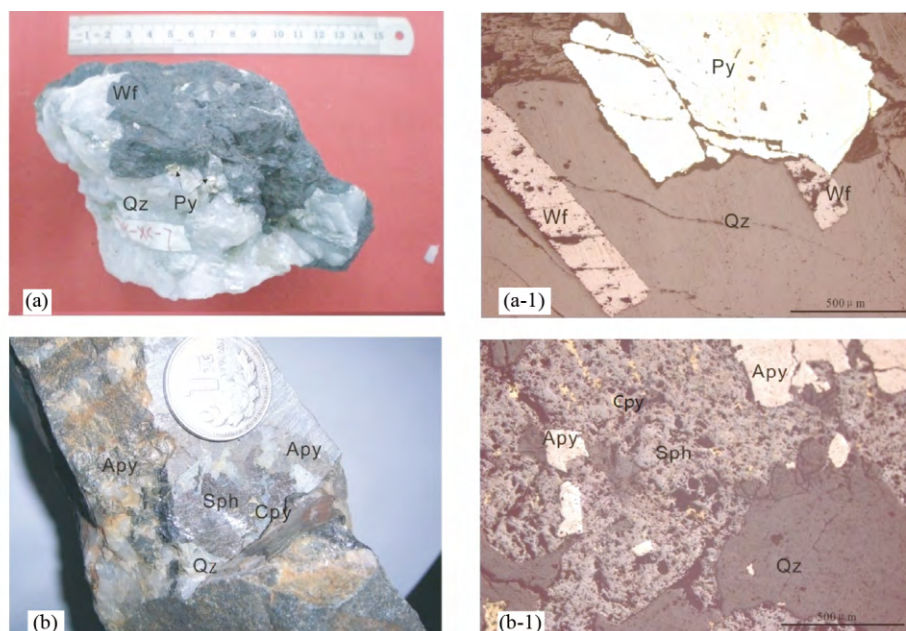


图2 陶锡坑钨矿床用于 He、Ar 同位素研究的黄铁矿和毒砂标本及显微照片

黑钨矿-石英组合矿石标本 (a) 及相应的显微照片 (a-1); 毒砂-闪锌矿-石英组合矿石标本 (b) 及相应的显微照片 (b-1). Apy-毒砂; Cpy-黄铜矿; Py-黄铁矿; Sph-闪锌矿; Wf-黑钨矿; Qz-石英

Fig. 2 Samples and micrographs of pyrite and arsenopyrite used in He and Ar isotopic studies from the Taoxikeng tungsten deposit

(295.5), $^{38}\text{Ar}/^{36}\text{Ar}$ 为 0.19 ~ 0.23, 平均 0.183, 与大气值 (0.188) 接近。

4 讨论

4.1 成矿流体的 He 同位素组成及其指示意义

矿物流体包裹体中的 He 除来自成矿时的热液流体外, 还可能受后期扩散丢失、后生叠加及同位素分馏的影响。但前人的研究表明, 当流体包裹体的寄主矿物是硫酸盐和硫化物时, 包裹体内的稀有气体被捕获后不会发生明显的扩散丢失 (Trull *et al.*, 1991; Jean-Baptiste and Fouquet, 1996; 胡瑞忠等, 1999; Hu *et al.*, 2004)。本次测试矿物为黄铁矿和毒砂, 因此可以排除后期扩散丢失的影响。根据 Craig and Lupton (1976) 的方法, 结合矿床实际情况, 以流体包裹体的铀含量为 2.7×10^{-6} , Th/U = 0 (Th 在热液中溶解度极低), 成矿时代为 160Ma 作为边界条件, 扣除流体包裹体形成之后的原地放射成因 ^4He , 扣除后的 $^3\text{He}/^4\text{He}$ 值在测试误差范围之内 (Craig and Lupton, 1976), 因此后生叠加的影响也可忽略不计。大量研究表明, 稀有气体不同于其他稳定同位素, 在流体包裹体捕获和提取过程中一般不会产生明显的同位素分馏 (Jean-Baptiste and Fouquet, 1996; 胡瑞忠等, 1999; Ballentine *et al.*, 2002; Podosek *et al.*, 1981)。因此, 本次测试黄铁矿和毒砂矿物中流体包裹体的稀有气体组成应该可以代表流体的初始组成。

地壳流体中稀有气体有饱和空气雨水、地幔流体和地壳

放射成因三个明显不同的源区。不同来源的氦、氩同位素组成及其特征比值具有显著差别 (Trull *et al.*, 1991; Turner *et al.*, 1993; Stuart *et al.*, 1995; Burnard *et al.*, 1999; Hu *et al.*, 1998, 2004, 2009, 2012)。He 在大气中的含量极低, 通常用参数 $F^4\text{He}$ 来判断 (Kendrick *et al.*, 2001) ($F^4\text{He} = (^4\text{He}/^{36}\text{Ar})_{\text{样品}} / (^4\text{He}/^{36}\text{Ar})_{\text{大气}}$, 其中, $(^4\text{He}/^{36}\text{Ar})_{\text{大气}} = 0.1655$)。若样品为大气氦, 则 $F^4\text{He} = 1$ 。由表 1 可知, 样品中 $F^4\text{He}$ 的值为 867.5 ~ 5856, 远远大于 1, 说明样品中大气 He 可忽略不计, 故成矿流体中的 He 只可能来自地壳和地幔两大源区。Ballentine *et al.* (2002) 认为, 流体中 $^3\text{He}/^4\text{He}$ 比值 $> 0.1\text{Ra}$ 就证明成矿流体中含幔源流体。本次测试结果显示, 样品的 $^3\text{He}/^4\text{He}$ 值在 0.37 ~ 2.11Ra 之间, 远高于地壳值 ($< 0.1\text{Ra}$), 但低于地幔值 (8 ~ 9Ra), 说明成矿流体中有部分地幔流体参与了成矿作用。从氦同位素组成演化图 (图 3) 和 $^{40}\text{Ar}/^{36}\text{Ar}$ - $^3\text{He}/^4\text{He}$ (图 4) 中也可以看出, $^3\text{He}/^4\text{He}$ 值分布在地壳与地幔的过渡带中, 说明成矿流体的 He 具有壳-幔混合来源的特征。

4.2 Ar 同位素的指示意义

毒砂流体包裹体的 $^{40}\text{Ar}/^{36}\text{Ar}$ 变化范围在 309.5 ~ 383.6; 黄铁矿流体包裹体中的 $^{40}\text{Ar}/^{36}\text{Ar}$ 变化范围在 323.4 ~ 338.7; 相较于大气降水的 $^{40}\text{Ar}/^{36}\text{Ar}$ 特征值 (295.5) 偏大, 说明流体中存在壳源或幔源的放射成因 Ar (Ar^*)。

由 Kendrick *et al.* (2001) 总结的放射性成因 $^{40}\text{Ar}^*$ 的比率, 即 $^{40}\text{Ar}_e$, 由以下公式计算:

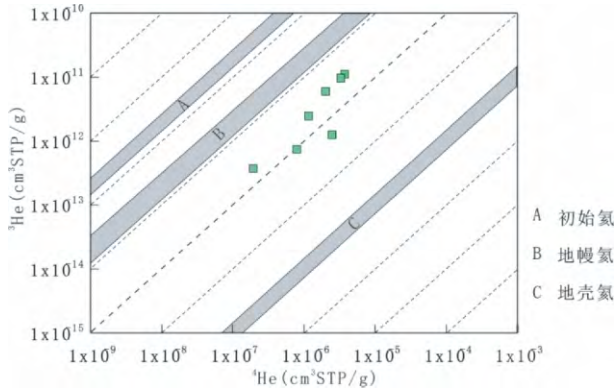


图3 淘锡坑钨矿床成矿流体 He 同位素组成图
Fig. 3 He isotope of ore-forming fluid in the Taoxikeng tungsten deposit

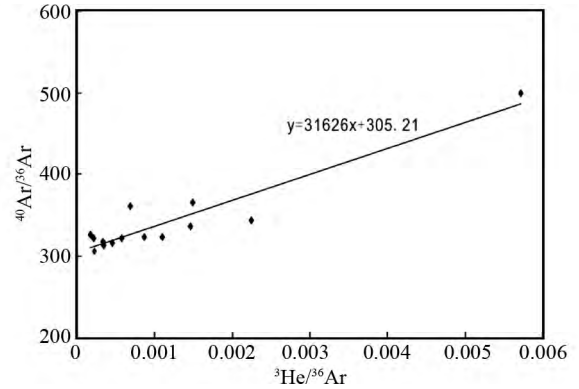


图5 淘锡坑钨矿床成矿流体 ³He/³⁶Ar-⁴⁰Ar/³⁶Ar 图解
Fig. 5 ³He/³⁶Ar vs. ⁴⁰Ar/³⁶Ar plot of ore-forming fluid in the Taoxikeng tungsten deposit

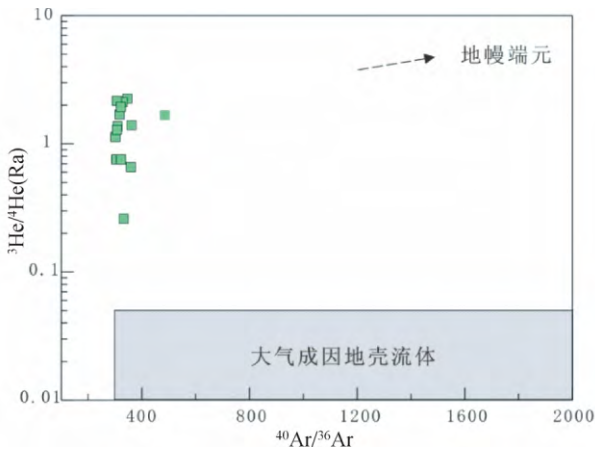


图4 淘锡坑钨矿床成矿流体 ⁴⁰Ar/³⁶Ar-³He/⁴He 图解
Fig. 4 ⁴⁰Ar/³⁶Ar vs. ³He/⁴He (Ra) plot of ore-forming fluid in the Taoxikeng tungsten deposit

$$^{40}\text{Ar}_E = \frac{(^{40}\text{Ar}/^{36}\text{Ar})_{\text{样品}} - 295.5}{(^{40}\text{Ar}/^{36}\text{Ar})_{\text{样品}}} \times 100\%$$

计算显示,样品中放射性成因 Ar* 的比率 (⁴⁰Ar_E) 为 4.5% ~ 12.3%,说明样品中大气 Ar 的贡献达到了 87.7% ~ 95.5%,成矿流体中 Ar 主要为大气 Ar。样品原位放射成因 ⁴⁰Ar 的贡献可忽略不计。说明成矿流体中 Ar 主要为大气 Ar。

根据 ³He/³⁶Ar 与 ⁴⁰Ar/³⁶Ar 的相关关系,用最小二乘法拟合,当 ³He/³⁶Ar = 5 × 10⁻⁸ (雨水的 ³He/³⁶Ar 值) 时,该矿床地壳流体端元的 ⁴⁰Ar/³⁶Ar 约为 305 (图 5),其值在误差范围内与大气饱和水的同位素组成 (⁴⁰Ar/³⁶Ar ≈ 295.5) 相似,过剩氦很少,此即该区成矿流体中具雨水性质的地壳端元。由表 1 和图 6 可知,该矿床地壳流体端元的 ⁴⁰Ar* /⁴He 比值为 0.036 ~ 0.09,远低于地壳岩石典型的 ⁴⁰Ar* /⁴He 值 (0.2) 和典型的地幔 ⁴⁰Ar* /⁴He 值 (0.25 ~ 0.5) (Allègre *et al.*, 1987; Stuart *et al.*, 1995; Graham, 2002; Burnard and Polya,

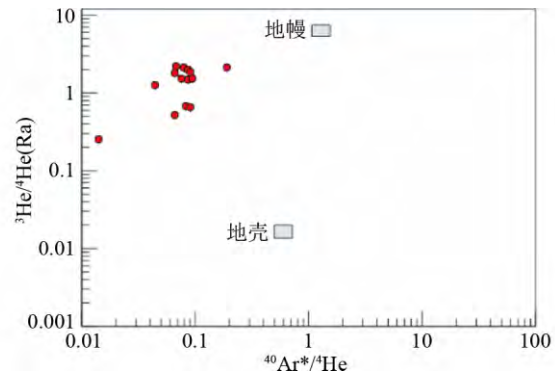


图6 淘锡坑钨矿床成矿流体 ⁴⁰Ar* /⁴He-³He/⁴He 图解
Fig. 6 ⁴⁰Ar* /⁴He vs. ³He/⁴He (Ra) plot of ore-forming fluid in the Taoxikeng tungsten deposit

2004) 说明地壳端元流体具有特别低的 ⁴⁰Ar* /⁴He 值。已有研究表明,现代地下水 ⁴⁰Ar* /⁴He 值的降低,是地下水流经岩石优先获取 ⁴He (相对于 ⁴⁰Ar) 的结果 (Torgersen *et al.*, 1989)。地下水从地壳岩石中获取放射成因的 ⁴⁰Ar 和 ⁴He 与 Ar 和 He 的封闭温度有关 (Torgersen *et al.*, 1989; Ballentine *et al.*, 2002),对大多数矿物而言,He 的封闭温度往往低于 200℃,而 ⁴⁰Ar 的封闭温度往往高于 200℃ (Lippolt and Weigel, 1988; Elliot *et al.*, 1993),在 250℃ 时,Ar 可保存于大多数矿物中。因此,地壳端元流体对地壳岩石中氦的优先富集特性,说明地壳端元流体是一种低温 (<250℃) 大气成因地下水。

综上所述,淘锡坑钨矿床流体包裹体中 He、Ar 同位素组成表明,该成矿流体具有地幔与地壳两端元混合的特征。其中,壳源流体为地下循环的低温饱和和大气水。

4.3 成矿机制探讨

本次稀有气体研究表明,淘锡坑矿床成矿流体具壳幔混合的特点,进一步说明了地幔流体参与成矿作用。H、O、S 同

位素组成表明,成矿流体主要为岩浆流体,并有大气降水的加入(宋生琼等,2009,2011a,b)。前人研究表明,该矿床之下的隐伏花岗岩在成矿过程中可能为本矿床提供了成矿物质(邹欣,2006;宋生琼等,2011b;杨帆等,2014)。成岩成矿时代研究显示,隐伏花岗岩体的锆石 U-Pb 年龄为 $158.7 \pm 3.9\text{Ma}$ 和 $157.6 \pm 3.5\text{Ma}$ (郭春丽等,2007)。矿石中石英的 Rb-Sr 等时线年龄为 $161 \pm 4\text{Ma} \sim 154 \pm 4\text{Ma}$ (郭春丽等,2007;Guo *et al.*,2011);白云母 Ar-Ar 年龄为 $155 \pm 1.4\text{Ma} \sim 152.7 \pm 1.5\text{Ma}$ (郭春丽等,2008;Guo *et al.*,2011)。辉钼矿的 Re-Os 等时线年龄变化于 $156.4 \pm 3.5\text{Ma} \sim 153.5 \pm 2.2\text{Ma}$ (陈郑辉等,2006)。可见,成岩与成矿时代在误差范围内一致。已有研究显示,这一时期华南地区一些钨锡多金属矿床的成矿流体中有地幔组分存在。例如,湖南芙蓉锡矿的 $^3\text{He}/^4\text{He}$ 值为 $0.14 \sim 2.95\text{Ra}$ (Li *et al.*,2007),湖南柿竹园 W-Sn-Bi-Mo 矿床 $^3\text{He}/^4\text{He}$ 值为 $0.06 \sim 1.66\text{Ra}$ (Wu *et al.*,2011),湖南瑶岗仙 $^3\text{He}/^4\text{He}$ 值为 $0.58 \sim 3.03\text{Ra}$ (Hu *et al.*,2012),江西漂塘钨矿 $^3\text{He}/^4\text{He}$ 值为 $0.17 \sim 0.86\text{Ra}$ (Wang *et al.*,2010)。综合考虑上述研究成果,作者认为矿床成矿流体是花岗岩浆分异出的岩浆流体与大气成因地下水的混合作用形成,其中花岗岩的形成与地幔流体的参与密不可分。

以往研究表明,华南在中生代发生了一系列大规模的软流圈上涌、岩石圈减薄、地壳伸展等地球动力学过程(Xu *et al.*,1999;孙涛和周新民,2002;谢桂青等,2005)。结合 Hu *et al.*(2012)的研究结果,作者也认为上述动力学过程为来自深部的地幔流体上涌到中下地壳提供了通道,地幔流体带来的热引起地壳重熔形成花岗岩浆,并为重熔的花岗岩浆提供成矿物质,这种混合了地幔流体的花岗岩浆沿有利构造侵入并分异演化,形成高温的富含地幔 He 等挥发份的含矿热液,向顶部和边部相对开放的构造裂隙中富集。而开放的构造裂隙中存在大量低温大气降水。这使得高温含矿流体与低温大气降水发生混合作用,大量成矿物质析出形成该矿床。

5 结论

(1) 陶锡坑钨多金属矿床成矿流体的 $^3\text{He}/^4\text{He}$ 值为 $0.37 \sim 2.11\text{Ra}$, $^{40}\text{Ar}/^{36}\text{Ar}$ 值为 $309.5 \sim 383.6$,成矿流体具有壳-幔两端元混合的特征。其中,地壳端元为经过地下循环的低温饱和和大气水,含地幔组分的端元为隐伏花岗岩体成岩过程中分异出的岩浆流体。

(2) 该矿床的形成与华南在中生代发生的大规模软流圈上涌、岩石圈减薄、地壳伸展等地球动力学背景密切相关。这种动力学过程为地幔流体带来的热引起地壳重熔形成成矿花岗岩浆提供了条件,同时地幔流体参与了花岗岩的重熔作用。

致谢 胡瑞忠研究员、武丽艳副研究员在本文写作过程中

给予了悉心指导和大力帮助,在此表示感谢。

References

- Allègre CJ, Staudacher T and Sarda P. 1987. Rare gas systematics: Formation of the atmosphere, evolution and structure of the earth's mantle. *Earth and Planetary Science Letters*, 81(2-3): 127-150
- Ballentine CJ, Burgess R and Marty B. 2002. Tracing fluid origin, transport and interaction in the crust. *Reviews in Mineralogy and Geochemistry*, 47(1): 539-614
- Burnard PG, Hu R, Turner G and Bi XW. 1999. Mantle, crustal and atmospheric noble gases in Ailaoshan gold deposits, Yunnan Province, China. *Geochimica et Cosmochimica Acta*, 63(10): 1595-1604
- Burnard PG and Polya DA. 2004. Importance of mantle derived fluids during granite associated hydrothermal circulation: He and Ar isotopes of ore minerals from Panasqueira. *Geochimica et Cosmochimica Acta*, 68(7): 1607-1615
- Chen ZH, Wang DH, Qu WJ, Chen YC, Wang PA, Xu JX, Zhang JJ and Xu ML. 2006. Geological characteristics and mineralization age of the Taoxikeng tungsten deposit in Chongyi County, southern Jiangxi Province, China. *Geological Bulletin of China*, 25(4): 496-501 (in Chinese with English abstract)
- Chi GX and Lai JQ. 2009. Roles of fluid inclusions in study of mineral deposits. *Mineral Deposits*, 28(6): 850-855 (in Chinese with English abstract)
- Craig H and Lupton JE. 1976. Primordial neon, helium, and hydrogen in oceanic basalts. *Earth and Planetary Science Letters*, 31(3): 369-385
- Elliot T, Ballentine CJ, O'Nions RK and Ricchiuto T. 1993. Carbon, helium, neon and argon isotopes in a Po Basin (Northern Italy) natural gas field. *Chemical Geology*, 106(3-4): 429-440
- Feng CY, Feng YD, Xu JX, Zeng ZL, She HQ, Zhang DQ, Qu WJ and Du AD. 2007. Isotope chronological evidence for Upper Jurassic petrogenesis and mineralization of altered granite-type tungsten deposits in the Zhangtiantang area, southern Jiangxi. *Geology in China*, 34(4): 642-650 (in Chinese with English abstract)
- Graham DW. 2002. Noble gas isotope geochemistry of mid-ocean ridge and ocean island basalts: Characterization of mantle source reservoirs. *Reviews in Mineralogy and Geochemistry*, 47(1): 247-317
- Graupner T, Kempe U, Dombon E, Pätzold O, Leeder O and Spooner ETC. 1999. Fluid regime and ore formation in the tungsten (yttrium) deposits of Kyzyltau (Mongolian Altai): Evidence for fluid variability in tungsten-tin ore systems. *Chemical Geology*, 154(1-4): 21-58
- Graupner T, Bray CJ, Spooner ETC and Herzig PM. 2001. Analysis of fluid inclusions in seafloor hydrothermal precipitates: Testing and application of an integrated GC/IC technique. *Chemical Geology*, 177(3-4): 443-470
- Guo CL, Wang DH, Chen YC, Wang YB, Chen ZH and Liu SB. 2007. Precise zircon SHRIMP U-Pb and quartz vein Rb-Sr dating of Mesozoic Taoxikeng tungsten polymetallic deposit in southern Jiangxi. *Mineral deposits*, 26(4): 432-442 (in Chinese with English abstract)
- Guo CL, Lin ZY, Wang DH, Chen W, Zhang Y, Feng CY, Chen ZH, Zeng ZL and Cai RQ. 2008. Petrologic characteristics of the granites and greisens and muscovite $^{40}\text{Ar}/^{39}\text{Ar}$ dating in the Taoxikeng tungsten polymetallic deposit, southern Jiangxi Province. *Acta Geologica Sinica*, 82(9): 1274-1284 (in Chinese with English abstract)
- Guo CL, Mao JW, Bierlein F, Chen ZH, Chen YC, Li CB and Zeng ZL. 2011. Shrimp U-Pb (zircon), Ar-Ar (muscovite) and Re-Os (molybdenite) isotopic dating of the Taoxikeng tungsten deposit, South China Block. *Ore Geology Reviews*, 43(1): 26-39
- Hu RZ, Burnard PG, Turner G and Bi XW. 1998. Helium and Argon

- isotope systematics in fluid inclusions of Machangqing copper deposit in West Yunnan Province, China. *Chemical Geology*, 146(1–2): 55–63
- Hu RZ, Bi XW, Turner G and Burnard PG. 1999. He and Ar isotopic geochemistry of gold ore-forming fluids in the Ailaoshan gold mineralization belt. *Science in China (Series D)*, 29(4): 321–330 (in Chinese)
- Hu RZ, Burnard PG, Bi XW, Zhou MF, Pen JT, Su WC and Wu KX. 2004. Helium and argon isotope geochemistry of alkaline intrusion-associated gold and copper deposits along the Red River–Jinshajiang fault belt, SW China. *Chemical Geology*, 203(3–4): 305–317
- Hu RZ, Burnard PG, Bi XW, Zhou MF, Peng JT, Su WC and Zhao JH. 2009. Mantle-derived gaseous components in ore-forming fluids of the Xiangshan uranium deposit, Jiangxi Province, China: Evidence from He, Ar and C isotopes. *Chemical Geology*, 266(1–2): 86–95
- Hu RZ and Zhou MF. 2012. Multiple Mesozoic mineralization events in South China: An introduction to the thematic issue. *Mineralium Deposita*, 47(6): 579–588
- Hu RZ, Bi XW, Jiang GH, Chen HW, Peng JT, Qi YQ, Wu LY and Wei WF. 2012. Mantle-derived noble gases in ore-forming fluids of the granite-related Yaogangxian tungsten deposit, southeastern China. *Mineralium Deposita*, 47(6): 623–632
- Hu RZ, Mao JW, Hua RM and Fan WM. 2015. Intra-Continental Mineralization of South China Craton. Beijing: Science Press, 1–903 (in Chinese)
- Jean-Baptiste P and Fouquet Y. 1996. Abundance and isotopic composition of helium in hydrothermal sulfides from the East Pacific Rise at 13°N. *Geochimica et Cosmochimica Acta*, 60(1): 87–93
- Kendrick MA, Burgess R, Patrick RAD and Turner G. 2001. Fluid inclusion noble gas and Halogen evidence on the origin of Cu-porphphy mineralizing fluids. *Geochimica et Cosmochimica Acta*, 65(16): 2651–2668
- Li ZL, Hu RZ, Yang JS, Peng JT, Li XM and Bi XW. 2007. He, Pb and S isotopic constraints on the relationship between the A-type Qitianling granite and the Furong tin deposit, Hunan Province, China. *Lithos*, 97(1–2): 161–173
- Lippolt HJ and Weigel E. 1988. ⁴He diffusion in ⁴⁰Ar-retentive minerals. *Geochimica et Cosmochimica Acta*, 52(6): 1449–1458
- Liu YM, Wang CL, Xue YZ, Lu HZ, Kang WQ and Zeng T. 1998. Metallogenic conditions and metallogenic models of Shizhuyuan ultra-large tungsten polymetallic deposit. *Science in China (Series D)*, 28(Suppl.): 49–56 (in Chinese)
- Lu HZ, Fang HR, Nie P, Ou GX, Shen K and Zhang WH. 2004. Fluid Inclusion. Beijing: Science Press, 1–487 (in Chinese)
- Ma TQ, Wu GY, Jia BH, Bai DY, Wang XH and Chen BH. 2005. Middle-Late Jurassic granite magma-mixing in the middle segment of the Nanling Mountains, South China: Evidence from mafic microgranular enclaves. *Geological Bulletin of China*, 24(6): 506–512 (in Chinese with English abstract)
- Mao JW, Xie GQ, Li XF, Zhang CQ and Mei YX. 2004. Mesozoic large scale mineralization and multiple lithospheric extension in South China. *Earth Science Frontiers*, 11(1): 45–55 (in Chinese with English abstract)
- Mao JW, Cheng YB, Chen MH and Pirajno F. 2013. Major types and time-space distribution of Mesozoic ore deposits in South China and their geodynamic settings. *Mineralium Deposita*, 48(3): 267–294
- Paradis S, Chi G and Lavoie D. 2004. Fluid inclusion and isotope evidence for the origin of the Upton Ba-Zn-Pb deposit, Quebec Appalachians, Canada. *Economic Geology*, 99(4): 807–817
- Podosek FA, Bernatowicz TJ and Kramer FE. 1981. Adsorption of xenon and krypton on shales. *Geochimica et Cosmochimica Acta*, 45(12): 2401–2415
- Roedder E. 1984. Fluid inclusions. *Reviews in Mineralogy and Geochemistry*, 12: 644
- Song SQ, Hu RZ, Bi XW, Wei WF and Shi SH. 2009. Hydrogen, oxygen and sulfur isotope geochemical characteristics of Taoxikeng tungsten deposit in Chongyi County, southern Jiangxi Province. *Acta Mineralogica Sinica*, (Suppl.): 328 (in Chinese)
- Song SQ, Hu RZ, Bi XW, Wei WF and Shi SH. 2011a. Fluid inclusion geochemistry of the Taoxikeng tungsten deposit in southern Jiangxi Province, China. *Geochimica*, 40(3): 237–248 (in Chinese with English abstract)
- Song SQ, Hu RZ, Bi XW, Wei WF and Shi SH. 2011b. Hydrogen, oxygen and sulfur isotope geochemical characteristics of Taoxikeng tungsten deposit in Chongyi County, southern Jiangxi Province. *Mineral Deposits*, 30(1): 1–10 (in Chinese with English abstract)
- Stuart FM, Burnard PG, Taylor RP and Turner G. 1995. Resolving mantle and crustal contributions to ancient hydrothermal fluids: He–Ar isotopes in fluid inclusions from Dae Hwa W–Mo mineralisation, South Korea. *Geochimica et Cosmochimica Acta*, 59(22): 4663–4673
- Sun T and Zhou XM. 2002. Late Mesozoic extension in Southeast China: Petrologic symbols. *Journal of Nanjing University (Natural Science)*, 38(6): 737–746 (in Chinese with English abstract)
- Torgersen T and Jenkins WJ. 1982. Helium isotopes in geothermal systems: Iceland, the geysers, Raft River and steamboat springs. *Geochimica et Cosmochimica Acta*, 46(5): 739–748
- Torgersen T, Kennedy BM, Hiyagon H, Chiou KY, Reynolds JH and Clarke WB. 1989. Argon accumulation and the crustal degassing flux of ⁴⁰Ar in the Great Artesian basin, Australia. *Earth and Planetary Science Letters*, 92(1): 43–56
- Trull T, Kurz MD and Jenkins WI. 1991. Diffusion of cosmogenic ³He in olivine and quartz: Implications for surface exposure dating. *Earth and Planetary Science Letters*, 103(1–4): 241–256
- Tu GC. 1998. The unique nature in ore composition, geological background and metallogenic mechanism of non-conventional superlarge ore deposits: A preliminary discussion. *Science in China (Series D)*, 41(Suppl.): 1–6
- Turner G, Burnard P, Ford JL, Gilmour JD, Lyon IC and Stuart FM. 1993. Tracing fluid sources and interactions. *Philosophical Transactions of the Royal Society of London Series A: Mathematical Physical and Engineering Sciences*, 344(1670): 127–140
- Wang XD, Ni P, Jiang SY, Zhao KD and Wang TG. 2010. Origin of ore-forming fluid in the Piaotang tungsten deposit in Jiangxi Province: Evidence from Helium and argon isotopes. *Chinese Science Bulletin*, 55(7): 628–634
- Wei SL, Jia BH and Zeng QW. 2006. Metallogenic mechanism of tungsten deposit in Nanling area. *Resources Survey & Environment*, 27(2): 103–109 (in Chinese with English abstract)
- Wilkinson JJ. 2001. Fluid inclusions in hydrothermal ore deposits. *Lithos*, 55(1–4): 229–272
- Wu LY, Hu RZ, Peng JT, Bi XW, Jiang GH, Chen HW, Wang QY and Liu YY. 2011. He and Ar isotopic compositions and genetic implications for the giant Shizhuyuan W–Sn–Bi–Mo deposit, Hunan Province, South China. *International Geology Review*, 53(5–6): 677–690
- Wu YB and Zheng YF. 2013. Tectonic evolution of a composite collision orogen: An overview on the Qinling–Tongbai–Hong’an–Dabie–Sulu orogenic belt in central China. *Gondwana Research*, 23(4): 1402–1428
- Wu ZJ, Xu ML, Zhao L, Luo XH and Wu ST. 2009. The structural ore-controlled mechanism of the large-scaled Taoxikeng tungsten ore. *China Tungsten Industry*, 24(1): 16–20, 39 (in Chinese with English abstract)
- Xi BB, Zhang DH, Zhou LM, Zhang WH and Wang C. 2008. Characteristics of ore-forming fluid evolution in Dajishan tungsten deposit, Quannan County, Jiangxi. *Acta Geologica Sinica*, 82(7): 956–966 (in Chinese with English abstract)
- Xie GQ, Mao JW, Hu RZ, Li RL and Cao JJ. 2005. Discussion on some problems of Mesozoic and Cenozoic geodynamics of Southeast China. *Geological Review*, 51(6): 613–620 (in Chinese with English abstract)
- Xu ML, Feng WD, Zhang FR, Li JD and Luo XH. 2006. Metallogenic characteristics of Taoxikeng wolfram deposit, Chongyi. *Resources*

- Survey & Environment, 27(2): 159-163 (in Chinese with English abstract)
- Xu XS, Dong CW, Li WX and Zhou XM. 1999. Late Mesozoic intrusive complexes in the coastal area of Fujian, SE China: The significance of the gabbro-diorite-granite association. *Lithos*, 46(2): 299-315
- Yang F, Xiao RG, Bai FJ and Liang T. 2014. REE geochemistry of the Taoxikeng tungsten deposit in Ganzhou, Jiangxi Province. *Geology and Exploration*, 49(6): 1139-1152 (in Chinese with English abstract)
- Yu JH, Zhou XM, O'Reilly YS, Zhao L, Griffin WL, Wang RC, Wang LJ and Chen XM. 2005. Formation history and protolith characteristics of granulite facies metamorphic rock in Central Cathaysia deduced from U-Pb and Lu-Hf isotopic studies of single zircon grains. *Chinese Science Bulletin*, 50(18): 2080-2089
- Yuan SD, Peng JT, Hu RZ, Li HM, Shen NP and Zhang DL. 2008. A precise U-Pb age on cassiterite from the Xianghualing tin-polymetallic deposit (Hunan, South China). *Mineralium Deposita*, 43(4): 375-382
- Yuan SD, Peng JT, Hao S, Li HM, Geng JZ and Zhang DL. 2011. In situ LA-MC-ICP-MS and ID-TIMS U-Pb geochronology of cassiterite in the giant Furong tin deposit, Hunan Province, South China: New constraints on the timing of tin-polymetallic mineralization. *Ore Geology Reviews*, 43(1): 235-242
- Yuan SD, Mao JW, Cook NJ, Wang XD, Liu XF and Yuan YB. 2015. A Late Cretaceous tin metallogenic event in Nanling W-Sn metallogenic province: Constraints from U-Pb, Ar-Ar geochronology at the Jiepiling Sn-Be-F deposit, Hunan, China. *Ore Geology Reviews*, 65: 283-293
- Zhang SB and Zheng YF. 2013. Formation and evolution of Precambrian continental lithosphere in South China. *Gondwana Research*, 23(4): 1214-1260
- Zhang WL, Hua RM, Wang RC, Chen PR and Li HM. 2006. New dating of the Dajishan granite and related tungsten mineralization in southern Jiangxi. *Acta Geologica Sinica*, 80(7): 956-962 (in Chinese with English abstract)
- Zhao ZH, Bao ZW, Zhang BY and Xiong XL. 2001. Crust-mantle interaction and its contribution to the Shizhuyuan superlarge tungsten polymetallic mineralization. *Science in China (Series D)*, 44(3): 266-276
- Zou X. 2006. The research on the geochemical characteristic and genesis of tungsten deposit in Taoxikeng, Jiangxi. Master Degree Thesis. Beijing: China University of Geosciences, 1-60 (in Chinese)
- 宋生琼, 胡瑞忠, 毕献武, 魏文凤, 石少华. 2009. 赣南崇义地区钨锡坑钨矿氢、氧、硫同位素地球化学研究. *矿物学报*, (增刊): 328
- 宋生琼, 胡瑞忠, 毕献武, 魏文凤, 石少华. 2011a. 赣南钨锡坑钨矿床流体包裹体地球化学研究. *地球化学*, 40(3): 237-248
- 宋生琼, 胡瑞忠, 毕献武, 魏文凤, 石少华. 2011b. 赣南崇义钨锡坑钨矿床氢、氧、硫同位素地球化学研究. *矿床地质*, 30(1): 1-10
- 孙涛, 周新民. 2002. 中国东南部晚中生代伸展应力体制的岩石学标志. *南京大学学报(自然科学)*, 38(6): 737-746
- 涂光灿. 1998. 试论非常规超大型矿床物质组成、地质背景、形成机制的某些独特性-初谈非常规超大型矿床. *中国科学(D辑)*, 28(增刊): 1-6
- 魏绍六, 贾宝华, 曾钦旺. 2006. 南岭地区钨矿成矿机理探讨. *资源调查与环境*, 27(2): 103-109
- 吴至军, 徐敏林, 赵磊, 罗仙华, 邬思涛. 2009. 江西钨锡坑大型钨矿构造控矿机制探讨. *中国钨业*, 24(1): 16-20, 39
- 席斌斌, 张德会, 周利敏, 张文淮, 王成. 2008. 江西省全南县大吉山钨矿成矿流体演化特征. *地质学报*, 82(7): 956-966
- 谢桂青, 毛景文, 胡瑞忠, 李瑞玲, 曹建勤. 2005. 中国东南部-新生代地球动力学背景若干问题的探讨. *地质论评*, 51(6): 613-620
- 徐敏林, 冯卫东, 张凤荣, 李江东, 罗仙华. 2006. 崇义钨锡坑钨矿成矿地质特征. *资源调查与环境*, 27(2): 159-163
- 杨帆, 肖荣阁, 白凤军, 梁涛. 2014. 江西赣州钨锡坑钨矿床稀土地球化学研究. *地质与勘探*, 49(6): 1139-1152
- 张文兰, 华仁民, 王汝成, 陈培荣, 李惠民. 2006. 赣南大吉山花岗岩成岩与钨矿成矿年龄的研究. *地质学报*, 80(7): 956-962
- 赵振华, 包志伟, 张伯友, 熊小林. 2000. 柿竹园超大型钨多金属矿床形成的壳幔相互作用背景. *中国科学(D辑)*, 30(增刊): 161-168
- 邹欣. 2006. 江西钨锡坑钨矿地球化学特征及成因研究. 硕士学位论文. 北京: 中国地质大学, 1-60

附中文参考文献

- 陈郑辉, 王登红, 屈文俊, 陈毓川, 王平安, 许建祥, 张家菁, 许敏林. 2006. 赣南崇义地区钨锡坑钨矿的地质特征与成矿时代. *地质通报*, 25(4): 496-501
- 池国祥, 赖健清. 2009. 流体包裹体在矿床研究中的作用. *矿床地质*, 28(6): 850-855
- 丰成友, 丰耀东, 许建祥, 曾载淋, 余宏全, 张德全, 屈文俊, 杜安道. 2007. 赣南张天堂地区岩体型钨矿晚侏罗世成岩成矿的同位素年代学证据. *中国地质*, 34(4): 642-650
- 郭春丽, 王登红, 陈毓川, 王彦斌, 陈郑辉, 刘善宝. 2007. 赣南中生代钨锡坑钨矿区花岗岩锆石 SHRIMP 年龄及石英脉 Rb-Sr 年龄测定. *矿床地质*, 26(4): 432-442
- 郭春丽, 简志永, 王登红, 陈文, 张彦, 丰成友, 陈郑辉, 曾载淋, 蔡汝青. 2008. 赣南钨锡坑钨多金属矿床花岗岩和云英岩岩石特征及云英岩中白云母⁴⁰Ar/³⁹Ar 定年. *地质学报*, 82(9): 1274-1284
- 胡瑞忠, 毕献武, Turner G, Burnard P. 1999. 哀牢山金矿带金成矿